

# Hexagonal flow $v_6$ as a superposition of elliptic $v_2$ and triangular $v_3$ flows

L. Bravina,<sup>1</sup> B.H. Bruscheim Johansson,<sup>1,\*</sup> G. Eyyubova,<sup>2</sup> V.L. Korotkikh,<sup>2</sup> I.P. Lokhtin,<sup>2</sup>  
L.V. Malinina,<sup>2,†</sup> S.V. Petrushanko,<sup>2</sup> A.M. Snigirev,<sup>2</sup> and E.E. Zabrodin<sup>1,‡</sup>

<sup>1</sup> *Department of Physics, University of Oslo, PB 1048 Blindern, N-0316 Oslo, Norway*

<sup>2</sup> *Skobeltsyn Institute of Nuclear Physics, Moscow State University, RU-119991 Moscow, Russia*

(Dated: April 28, 2019)

Partial contributions of elliptic  $v_2$  and triangular  $v_3$  flows to the hexagonal  $v_6$  flow are studied within the HYDJET++ model for Pb+Pb collisions at  $\sqrt{s} = 2.76A$  TeV. Scaling of the ratio  $v_6^{1/6}\{\Psi_2\}/v_2^{1/2}\{\Psi_2\}$  in the elliptic flow plane,  $\Psi_2$ , is predicted in the range  $1 \leq p_t \leq 4$  GeV/ $c$  for semicentral and semiperipheral collisions. Jets increase this ratio by about 10% and also cause its rise at  $p_t \geq 3.5$  GeV/ $c$ . The part of  $v_6$  coming from  $v_2$  is instantly increasing as the reaction becomes more peripheral, whereas the contribution of  $v_3$  to  $v_6$  drops. This behavior explains the experimentally observed increase of correlations between second and sixth harmonics and the decrease of correlations between third and sixth harmonics with rising impact parameter  $b$ . Our study favors the idea that basic features of the hexagonal flow can be understood in terms of the interplay of elliptic and triangular flows.

PACS numbers: 25.75.-q, 25.75.Ld, 24.10.Nz, 25.75.Bh

## I. INTRODUCTION

One of the main goals of heavy-ion experiments at ultrarelativistic energies is the study of properties of a new state of matter, quark-gluon plasma (QGP). Collider experiments with gold-gold collisions at  $\sqrt{s} = 200$  GeV at the Relativistic Heavy Ion Collider (RHIC) provided a lot of evidence that a hot and dense substance formed at the very beginning of the collision could be treated as a nearly perfect fluid [1]. Therefore, the whole paradigm has been changed. The plasma is no longer believed to be an ideal gas of noninteracting (or weakly interacting) partons, but rather a strongly interacting liquid [2]. It demonstrates a strong degree of collectivity, and the transverse flow of hadrons, particularly *elliptic* flow [3], is a very important signal that supports the hydrodynamic description of heavy-ion collisions. Hydrodynamic models, however, overestimate the flow at  $p_t \geq 2$  GeV/ $c$  [4], whereas conventional microscopic transport models usually undermine the strength of elliptic flow either at midrapidity [5] or at high transverse momenta [6, 7] at energies of RHIC or higher. The best description of the flow signal is obtained, therefore, in hybrid models, such as VISHNU [8] and MUSIC [9], which couple hydrodynamic treatment of the early stage of the expansion to hadron cascade model as an afterburner.

At present, the flow analysis is based on a Fourier decomposition of the azimuthal distribution of hadrons

[10, 11],

$$E \frac{d^3N}{d^3p} = \frac{1}{\pi} \frac{d^2N}{dp_t^2 dy} \left[ 1 + 2 \sum_{n=1}^{\infty} v_n \cos n(\phi - \Psi_n) \right], \quad (1)$$

where  $\phi$  is the azimuthal angle between the transverse momentum of the particle and the participant event plane, each having its own azimuth  $\Psi_n$ , and  $p_t$  and  $y$  are the transverse momentum and the rapidity, respectively. The flow harmonic coefficients

$$v_n = \langle \cos n(\phi - \Psi_n) \rangle \quad (2)$$

are obtained by averaging over all events and all particles in each event. The first two harmonics, dubbed *directed*,  $v_1$ , and *elliptic*,  $v_2$ , flow have been studied rather intensively during the past 15 years [4], whereas the systematic study of higher harmonics, namely, *triangular*,  $v_3$ , *quadrangular* (or *hexadecapole*),  $v_4$ , *pentagonal*,  $v_5$ , and *hexagonal*,  $v_6$ , flow began quite recently in the Large Hadron Collider (LHC) era [12].

It is generally assumed that, in the case of noncentral collision of two similar nuclei, remnants of the interacting nuclei fly away quickly, thus giving space for expansion of the overlapped volume. In the transverse plane this area resembles an ellipse; therefore, odd harmonics of anisotropic flow, such as  $v_3$ ,  $v_5$ , etc., can be neglected because of the symmetry considerations. The concept of participant triangularity due to initial-state fluctuations was first introduced in [13]. In model simulations, the triangular flow signal was found to be directly proportional to the participant triangularity. After that, correlations were studied between the higher-order harmonic eccentricity coefficients  $\varepsilon_n$ , linked to participant plane angles  $\Phi_n$ , and the final anisotropic flow coefficients  $v_n$  and their final anisotropic flow angles  $\Psi_n$ ; see, e.g., [14–18]. This analysis was done within both ideal and viscous relativistic hydrodynamics with Monte Carlo–Glauber

\*Also at Oslo and Akershus University College of Applied Sciences (HIOA), Oslo, Norway

†Also at Joint Institute for Nuclear Researches, RU-141980 Dubna, Russia

‡Also at Skobeltsyn Institute of Nuclear Physics, Moscow State University, RU-119991 Moscow, Russia

or color glass condensate (CGC) initial conditions. One of the interesting observations is that just the first few flow harmonics survive after the hydrodynamic evolution despite the fact that the initial spacial anisotropies are of the same order [15]. The characteristic mode mixing between the different order flow coefficients has been revealed [16–18]. It is found that the final plane angles  $\Psi_n$ ,  $n > 3$  seem to be uncorrelated with the corresponding participant plane angles  $\Phi_n$ ,  $n > 3$ , associated with initial anisotropies [19]. In contrast, the response of the elliptic flow to ellipticity, as well as that of the triangular flow to triangularity, is approximately linear [17]. Is it because of the crosstalk of several harmonics, and which harmonics play a major role in this process? To answer these questions it would be important to study the influence of  $v_2$  and  $v_3$ , linked to elliptic and triangular anisotropies, respectively, on higher harmonics of the anisotropic flow. For our analysis the HYDJET++ model [20] is employed. The basic principles of the model are given in Sec. II.

## II. MODEL

The Monte Carlo event generator HYDJET++ is a superposition of two event generators, FASTMC [21, 22] and PYQUEN [23], describing soft and hard parts of particle spectra in ultrarelativistic heavy-ion collisions at energies from RHIC ( $\sqrt{s} = 200$  GeV) to LHC ( $\sqrt{s} = 5.5$  TeV). Both FASTMC and PYQUEN generate particles independently. Their partial contributions to the total event multiplicity depend on collision energy and centrality. The soft part of a single event in HYDJET++ is a thermal hadronic state treated within the framework of parametrized hydrodynamics [21, 22]. The hard part of this event is represented by a multiple scattering of hard partons in a hot and dense medium, such as quark-gluon plasma. It accounts for the radiative and collisional energy losses [24] and shadowing effect [25]. Further details of the HYDJET++ model can be found elsewhere [20–23]. Below we concentrate on the simulation of anisotropic flow in the recent version of HYDJET++ [26].

In the case of noncentral collisions of identical nuclei the overlap area has a characteristic almond shape. This ellipsoid possesses the initial coordinate anisotropy, which is a function of impact parameter  $b$  and nuclear radius  $R_A$ ,  $\epsilon_0(b) = b/(2R_A)$ . In the azimuthal plane the transverse radius of the fireball reads [22]

$$R_{\text{ell}}(b, \phi) = R_{\text{fo}}(b) \frac{\sqrt{1 - \epsilon^2(b)}}{\sqrt{1 + \epsilon(b) \cos 2\phi}}. \quad (3)$$

Here  $\phi$  is the azimuthal angle and  $R_{\text{fo}}(0)$  is the model parameter that determines the scale of the fireball transverse size at freeze-out. The pressure gradients are stronger in the direction of the short axis in the transverse plane. Thus, the initial spatial anisotropy is transformed into the momentum anisotropy, which results in

the anisotropy of the flow. The azimuthal angle of the fluid velocity vector  $\phi_{\text{fl}}$  is linked to the azimuthal angle  $\phi$  via [22]

$$\frac{\tan \phi_{\text{fl}}}{\tan \phi} = \sqrt{\frac{1 - \delta(b)}{1 + \delta(b)}}, \quad (4)$$

with  $\delta(b)$  being the flow anisotropy parameter. In the employed version of HYDJET++ both spatial and flow anisotropies,  $\epsilon(b)$  and  $\delta(b)$ , are proportional to the initial spatial anisotropy  $\epsilon_0 = b/(2R_A)$ .

To introduce the triangular flow the transverse radius of the freeze-out surface is modified further [cf. Eq. (10) from [14]]:

$$R(b, \phi) = R_{\text{ell}}(b, \phi) \{1 + \epsilon_3(b) \cos [3(\phi - \Psi_3)]\}, \quad (5)$$

where the new phase  $\Psi_3$  is randomly distributed with respect to the position of the reaction plane  $\Psi_2$ . It means, in particular, that the integrated triangular flow measured in the  $\Psi_2$  plane is zero, in accordance with the experimental observations. Similarly to  $\epsilon(b)$ , the new parameter  $\epsilon_3(b)$ , which is responsible for emergence of the triangular anisotropy, can be either linked to initial eccentricity  $\epsilon_0(b)$  or treated as a free parameter.

It is worth mentioning here several important points. Like many other hydrodynamic models, HYDJET++ does not consider directed flow; i.e.,  $v_1$  of particles is essentially zero. The model describes the midrapidity area of heavy-ion collisions rather than the fragmentation ones. Recent measurements of the directed flow of charged particles done by the ALICE Collaboration at midrapidity in lead-lead collisions at  $\sqrt{s} = 2.76$  TeV [27] show that  $v_1$  is order(s) of magnitude weaker than  $v_2$  and  $v_3$ . Then, in contrast to event-by-event (EeE) hydrodynamics, HYDJET++ has no evolution stage and, therefore, cannot trace, e.g., propagation of energy and density fluctuations of the initial state, the so-called hot spots. It deals already with the final components of anisotropic flow. Lacking the EeE fluctuations, the model-generated ratios of different flow harmonics could be directly confronted only with the ratios obtained from EeE analysis of the data. This is not the case, however, because the data on flow harmonics are averaged over the whole statistics before performing the analysis of ratios, such as  $v_n^{1/n}/v_2^{1/2}$ . It leads to acquiring an extra multiplier to which the model results (or data) should be adjusted; see [28] for details.

The elliptic flow of particles contributes to all even harmonics, i.e.,  $v_4$ ,  $v_6$ , etc. For instance, quadrangular flow in HYDJET++ is determined by the elliptic flow of particles, governed by hydrodynamics, and particles coming from jets [29, 30]. The interplay between the elliptic and triangular flows will result in the appearance of odd higher harmonics in the model. Similarly to  $v_2$ , triangular flow should contribute separately to  $v_6$ ,  $v_9$ , etc. The goal of our study of the hexagonal flow,  $v_6$ , is, therefore, twofold. First, the partial contributions of

$v_2$  and  $v_3$ , each having its own flow angle  $\Psi_2$  and  $\Psi_3$ , to  $v_6$  should be analyzed. Of particular interest are the features of the distributions  $v_6\{\Psi_2\}(p_t)$  and  $v_6\{\Psi_3\}(p_t)$ . Second, the model allows one to investigate the influence of nonflow correlations, arising from jet fragmentation and resonance decays, on the flow harmonics. The previous study [29, 30] of the  $v_4/v_2^2$  ratio revealed that the jet contribution to this ratio is quite substantial compared to the slight modification caused by the decays of resonances. But, before the analysis of generated spectra, we have to estimate individual contributions of elliptic and triangular flow to  $v_6$  within the framework of relativistic ideal hydrodynamics.

### III. $v_6$ AS A FUNCTION OF $v_2$ AND $v_3$

As was shown within the approach suggested in [31], the freeze-out distribution of fast particles obtained by a saddle-point integration is proportional to the exponential

$$\frac{d^3N}{dyd^2p_t} \propto \exp\left(\frac{p_t u_{\max} - m_t u_{\max}^0}{T}\right), \quad (6)$$

where  $u = (u^0, u_{\parallel}, u_{\perp})$  is the fluid 4-velocity,  $u_{\parallel} \equiv u_{\max}$ ,  $v_{\max} = u_{\max}^0/u_{\max}$ ,  $y$  is the rapidity,  $T$  is the temperature and  $m_t = \sqrt{m^2 + p_t^2}$  is the transverse mass of a particle. The method utilizes the fact that fast particles come from regions of the freeze-out hypersurface where the  $u_{\parallel}$ , which is parallel to the particle's transverse momentum  $\vec{p}_t$ , is close to its maximum value  $u_{\max}$  [31]. Assuming for the sake of simplicity a single event plane and expanding  $u_{\max}(\phi)$  in Fourier series, one gets

$$u_{\max}(\phi) = u_{\max} \left[ 1 + 2 \sum_{n=1}^{\infty} V_n \cos(n\phi) \right]. \quad (7)$$

Denoting

$$a = \frac{p_t - m_t v_{\max}}{T} u_{\max},$$

we obtain from Eqs. (1), (6), and (7)

$$\exp\left\{ a \left[ 1 + 2 \sum_{n=1}^{\infty} V_n \cos(n\phi) \right] \right\} = 1 + 2 \sum_{n=1}^{\infty} v_n \cos(n\phi). \quad (8)$$

Then, the expressions for the elliptic and triangular flows read

$$v_2 = aV_2 \equiv \frac{p_t - m_t v_{\max}}{T} u_{\max} V_2, \quad (9)$$

$$v_3 = aV_3 \equiv \frac{p_t - m_t v_{\max}}{T} u_{\max} V_3, \quad (10)$$

respectively. It is easy to see that the quadrangular flow depends on both  $V_2$  and  $V_4$ :

$$v_4 = \frac{1}{2} a^2 V_2^2 + aV_4. \quad (11)$$

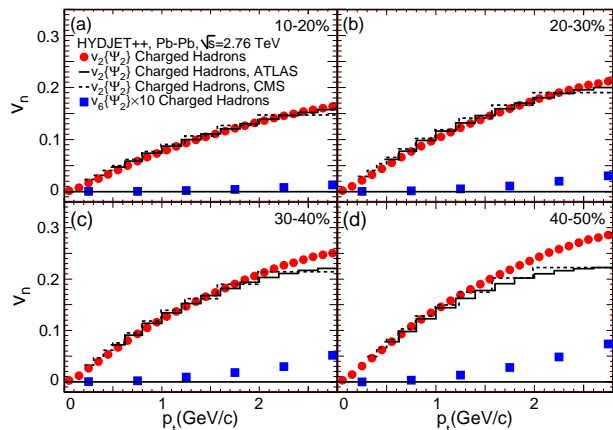


FIG. 1: (Color online) Transverse momentum dependencies of  $v_2\{\Psi_2\}$  (circles) and  $v_6\{\Psi_2\}$  (squares) of charged hadrons calculated within the HYDJET++ for Pb+Pb collisions at  $\sqrt{s} = 2.76$  TeV at centralities (a)  $\sigma/\sigma_{\text{geo}} = 10 - 20\%$ , (b)  $20 - 30\%$ , (c)  $30 - 40\%$ , and (d)  $40 - 50\%$ . Solid and dashed histograms show experimental data on  $v_2$  taken from ATLAS [32] and CMS [33], respectively.

Since the last term in Eq.(11)  $aV_4 \ll a^2V_2^2 \equiv v_2^2$  at  $p_t \rightarrow \infty$ , we regain the familiar result  $v_4 \cong \frac{1}{2}v_2^2$  [31]. For the hexagonal flow one gets, after the straightforward calculations,

$$v_6 = \frac{1}{6}(a^2V_2)^3 + \frac{1}{2}(aV_3)^2 + aV_6 + 3(aV_2)(aV_4). \quad (12)$$

Taking into account that at high transverse momenta  $aV_4 \ll v_2^2$  and  $aV_6 \ll a^2V_3^2 \equiv v_3^2$  we arrive at the simple expression

$$v_6 \cong \frac{1}{6}v_2^3 + \frac{1}{2}v_3^2. \quad (13)$$

Note again that this result was obtained under the assumption of a single event plane. We have learned in the past few years, however, that each of the flow harmonics  $v_n$  possesses its own event plane  $\Psi_n$  not necessarily coinciding with the others. The interplay between different event planes can be very important, and one should consider Eq. (13) as a first-order approximation. Model results for the hexagonal flow and its correlations with the elliptic and triangular flows are given below.

## IV. RESULTS AND DISCUSSION

To study the formation of the hexagonal flow in the model ca.  $2 \times 10^6$  lead-lead collisions were generated for each of four centralities  $\sigma/\sigma_{\text{geo}} = 10 - 20\%$ ,  $20 - 30\%$ ,  $30 - 40\%$ , and  $40 - 50\%$ . Transverse momentum distributions of  $v_6$  in  $\Psi_2$  and  $\Psi_3$  planes are shown in Figs. 1 and 2, respectively, together with the corresponding distributions for the elliptic and triangular flows. Available experimental data for  $v_2(p_t)$  and  $v_3(p_t)$  are plotted onto the

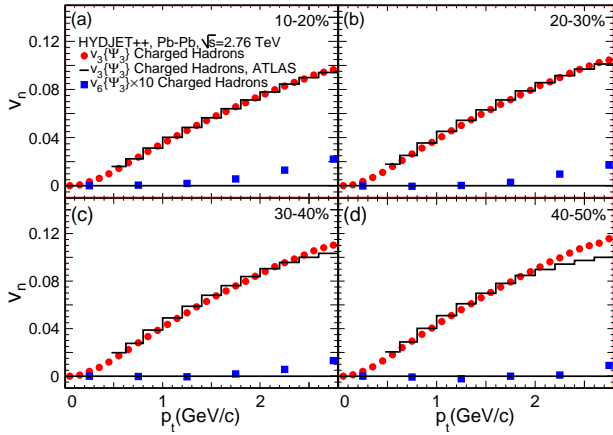


FIG. 2: (Color online) The same as Fig. 1 but for triangular and hexagonal flows in the  $\Psi_3$  plane. Histograms show experimental data on  $v_3$  taken from [32].

model calculations as well. The agreement with the data for both flow harmonics is fair. A detailed comparison of the model results with the data is given in [26]. Recall, that in contrast to many other hydrodynamic models the HYDJET++ model demonstrates a drop of elliptic flow at  $p_t \geq 3$  GeV/c [34, 35]. This drop is attributed in the model to the interplay of soft hydrodynamic processes and hard jets. In ideal hydrodynamics, particles with higher transverse momenta are carrying larger elliptic flow. However, the number of these particles decreases exponentially with rising  $p_t$ , and after certain  $p_t$  the particle spectrum is dominated by hadrons coming out from quenched jets. The elliptic flow of the jet hadrons is much lesser than the flow of hydro-induced hadrons; thus, the resulting flow of high- $p_t$  particles drops (to almost zero modulo path-length dependence of in-medium partonic energy loss).

It appears that the hexagonal flow in HYDJET++ is weak but not zero in both  $\Psi_2$  and  $\Psi_3$  planes. In the  $\Psi_2$  plane it starts to rise at  $p_t \geq 1.5$  GeV/c in semiperipheral collisions with  $\sigma/\sigma_{\text{geo}} \geq 30\%$ . Here we observe a clear tendency that  $v_6$  of charged hadrons with high transverse momenta increases with rising impact parameter. In the  $\Psi_3$  plane the high- $p_t$  tail of the distribution is presented as well. The generated  $v_6\{\Psi_3\}(p_t)$  seems to become a bit weaker at  $1 \leq p_t \leq 2.5$  GeV/c with increasing  $b$ , despite the fact that triangular flow slightly increases. This peculiarity is clarified in our study below.

To check the scaling trends in the behavior of different flow harmonics the ratio  $v_n^{1/n}/v_2^{1/2}$  is employed. The ratio  $v_6^{1/6}(p_t)/v_2^{1/2}(p_t)$  in the  $\Psi_2$  plane is displayed in Fig. 3 (a) for hadrons participated only in the hydrodynamic process and in Fig. 3(b) for all hadrons in the system. Note that the hexagonal flow here is determined with respect to  $\Psi_2$  plane and not its own  $\Psi_6$  plane. One can see the real scaling at  $p_t \geq 1$  GeV/c, where all curves are on top of each other. For “hydrodynamic” particles

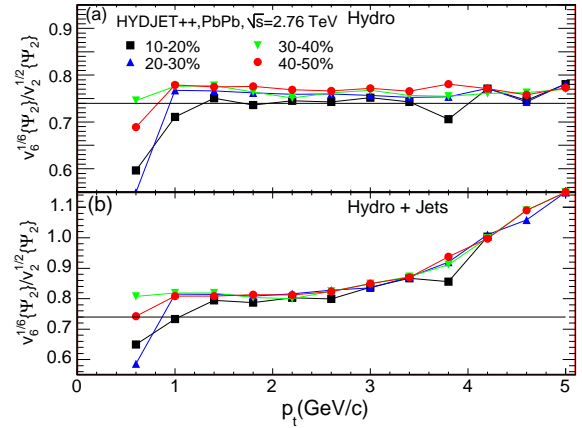


FIG. 3: (Color online) Ratio  $v_6^{1/6}/v_2^{1/2}$  as a function of  $p_t$  in the  $\Psi_2$  event plane for charged particles, originated from (a) soft processes only and (b) both soft and hard processes, in HYDJET++ simulations of Pb+Pb collisions at  $\sqrt{s} = 2.76$  TeV. The reaction centralities are 10 – 20% (squares), 20 – 30% (triangles pointing up), 20 – 30% (triangles pointing down), and 40 – 50% (circles). Solid lines in both plots show the prediction of ideal hydrodynamics for this ratio at high  $p_t$ , namely,  $v_6^{1/6}/v_2^{1/2} = (1/6)^{1/6} \approx 0.74$ .

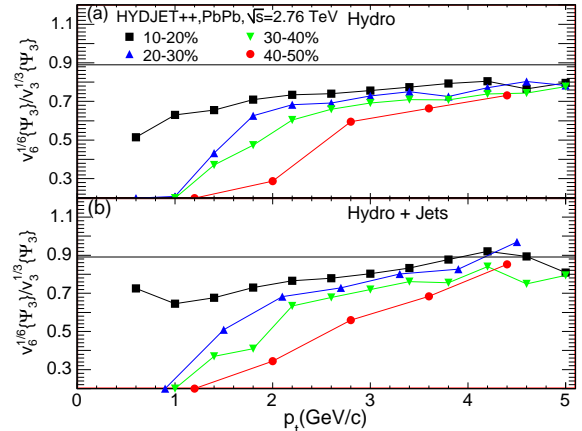


FIG. 4: (Color online) The same as Fig. 3 but for the ratio  $v_6^{1/6}/v_3^{1/3}$  vs.  $p_t$  in the  $\Psi_3$  event plane. Solid lines in both plots show the prediction of ideal hydrodynamics for this ratio at high  $p_t$ , namely,  $v_6^{1/6}/v_3^{1/3} = (1/2)^{1/6} \approx 0.89$ .

the relation  $v_6/v_3^3 \approx 1/6$  is fulfilled with good accuracy already at  $p_t = 1$  GeV/c. The effect of jets is twofold. First of all, hadrons from jets increase the considered ratio by  $\sim 10\%$  in the interval  $1 \leq p_t \leq 3$  GeV/c, as demonstrated in Fig. 3(b). Second, at larger transverse momenta the ratio starts to rise further in contrast to the plateau in the hydrodynamic case.

The situation with the ratio  $v_6^{1/6}(p_t)/v_3^{1/3}(p_t)$  in the  $\Psi_3$  plane, which is depicted in Fig. 4, is not so clear. This ratio is below the ideal high- $p_t$  limit  $v_6/v_3^3 \approx 1/2$ ,

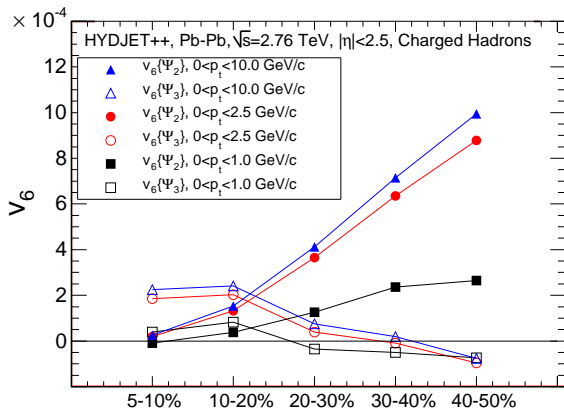


FIG. 5: (Color online) Hexagonal flow  $v_6\{\Psi_2\}$  and  $v_6\{\Psi_3\}$  of charged particles vs. centrality in Pb+Pb collisions at  $\sqrt{s} = 2.76$  TeV simulated by HYDJET++. The pseudorapidity interval is  $|\eta| < 2.5$ . Solid and open symbols indicate  $v_6\{\Psi_2\}$  and  $v_6\{\Psi_3\}$  of hadrons with transverse momenta below 10 GeV/c (triangles), 2.5 GeV/c (circles), and 1 GeV/c (squares), respectively.

but steadily increases to it with rising transverse momentum. Jets also increase this ratio and make its rise a bit steeper. In contrast to the scaling in the  $\Psi_2$  plane, the ratio  $v_6^{1/6}/v_3^{1/3}$  in the  $\Psi_3$  plane decreases for more peripheral collisions.

This means that the partial contributions of elliptic and triangular flows to the projections of the hexagonal flow onto  $\Psi_2$  and  $\Psi_3$  planes are changing with centrality. Figure 5 presents  $v_6$ , averaged in several  $p_t$  intervals, as a function of centrality in both  $\Psi_2$  and  $\Psi_3$  planes. Although the absolute magnitude of the signals depends on the selected  $p_t$  intervals, the tendencies in the  $v_6$  development are clearly revealed. Namely,  $v_6\{\Psi_2\}$  is weak in semicentral collisions but gradually increases for more peripheral reactions. This issue is supported by recent CMS data on hexagonal flow extracted by different methods [36]. And vice versa,  $v_6\{\Psi_3\}$  is maximal in semicentral collisions and then drops. Summarizing information provided by Eq. (13) and Figs. 1, 2, and 5, we arrive at the following scenario. For central topologies triangular flow is stronger than the elliptic one; therefore, it makes the main contribution to the hexagonal flow. The event plane  $\Psi_6$  is closer to the  $\Psi_3$  rather than the  $\Psi_2$  one. (Recall, that there are no genuine hexagonal deformations in the HYDJET++ model that can account for the formation of genuine  $v_6$ .) In peripheral topologies elliptic flow dominates over the triangular one. Thus, the resulting hexagonal flow event plane  $\Psi_6$  should be oriented closer to  $\Psi_2$ . In other words, in semicentral collisions  $\Psi_6$  is more strongly correlated with  $\Psi_3$ , whereas in more peripheral collisions  $\Psi_6$  is correlated with  $\Psi_2$ .

To see this interplay more distinctly, we apply the method of event plane correlators [37–39]. For each flow harmonic of  $n$ th order one has to determine the event

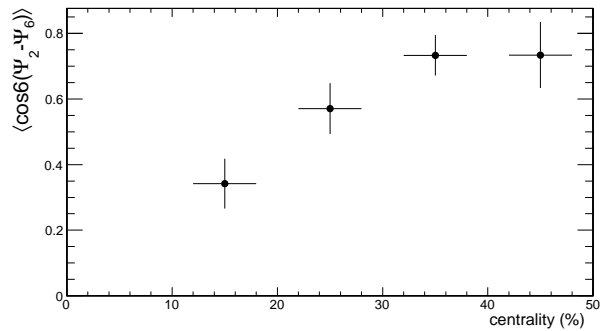


FIG. 6: Two-plane correlator  $\langle \cos 6(\Psi_2 - \Psi_6) \rangle$  as a function of centrality for charged hadrons in HYDJET++ simulated Pb+Pb collisions at  $\sqrt{s} = 2.76$  TeV.

flow vector  $\vec{Q}_n$  and the event plane angle  $\Psi_n$  following, e.g., prescription of [4, 11]

$$\begin{aligned} \vec{Q}_n &= (Q_{n,x}, Q_{n,y}) = \left( \sum_i w_i \cos(n\phi_i), \sum_i w_i \sin(n\phi_i) \right) \\ &= (Q_n \cos(n\Psi_n), Q_n \sin(n\Psi_n)) , \end{aligned} \quad (14)$$

$$\tan(n\Psi_n) = \frac{Q_{n,y}}{Q_{n,x}} , \quad (15)$$

where  $w_i$  and  $\phi_i$  are the weight and the azimuthal angle of the  $i$ th particle in the laboratory system, respectively. The correlators between arbitrary  $l$  event planes of order

$k_l$  have the form  $\langle \cos \left( \sum_{k=k_{l,\min}}^{k_{l,\max}} k C_k \Psi_k \right) \rangle$  with the constraint

$$\sum_{k=k_{l,\min}}^{k_{l,\max}} k C_k = 0. \quad \text{In our case of just two planes, } (\Psi_2, \Psi_6)$$

and  $(\Psi_3, \Psi_6)$ , the correlators are simply  $\langle \cos 6(\Psi_2 - \Psi_6) \rangle$  and  $\langle \cos 6(\Psi_3 - \Psi_6) \rangle$ , respectively. Both correlators were extracted from the HYDJET++ events by the method applied for analysis of experimental data [38]. This approach implies separation of a single event into two forward-backward symmetric subevents with a pseudorapidity gap in between, and takes into account resolution corrections for each of the event planes; see [38] for details and also [39] for generalization of the method. Moreover, to avoid ambiguity in the interpretation of the results, we artificially increased the triangularity of the freeze-out hypersurface. The obtained correlators are displayed in Figs. 6 and 7. In contrast to Fig. 5, here the correlations are investigated between the different event planes and not between the flow harmonics projected onto  $\Psi_2$  or  $\Psi_3$  planes. We see that the correlator  $\langle \cos 6(\Psi_2 - \Psi_6) \rangle$  increases for more peripheral collisions, whereas the correlator  $\langle \cos 6(\Psi_3 - \Psi_6) \rangle$  drops. Similar centrality dependencies were observed by the ATLAS Collaboration as well [38]. Such a behavior has a simple explanation. The event plane  $\Psi_6$  becomes closer to the  $\Psi_2$  one as the hexagonal flow is strongly determined by the  $v_2$  for the periph-

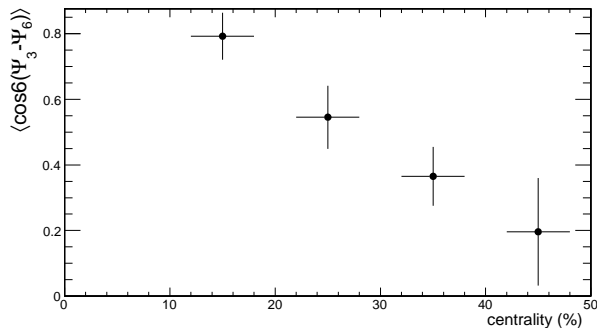


FIG. 7: The same as Fig. 6 but for two-plane correlator  $\langle \cos 6(\Psi_3 - \Psi_6) \rangle$ .

eral collisions. Because  $v_3$  is randomly oriented with respect to  $v_2$ , the correlations between the  $\Psi_6$  and the  $\Psi_3$  become weaker. Recently, various two- and many-plane correlators were studied in [39] within the microscopic a multiphase transport AMPT model. Very good agreement with the experiment is demonstrated. However, the authors attribute the drop of the correlations between the third and the sixth harmonics to the decrease of the triangular flow itself. This is not the case, because the magnitude of the  $v_3$  is approximately the same, as one can see, e.g., in Fig. 2. In our opinion, the falloff is driven by two reasons: (i) domination of  $v_2$  over  $v_3$  in semiperipheral and peripheral collisions, and (ii) absence of correlations between the  $\Psi_2$  and  $\Psi_3$ .

Finally, the contribution of the genuine hexagonal fluctuations to the final hexagonal flow should be weak. The experimentally observed event plane correlations and other features of  $v_6$  are reproduced in terms of interplay between the second and the third flow harmonics.

## V. CONCLUSIONS

The hexagonal flow  $v_6$  is studied within the HYDJET++ model in Pb+Pb collisions at  $\sqrt{s} = 2.76$  TeV

and centralities  $10\% \leq \sigma/\sigma_{\text{geo}} \leq 50\%$ . In contrast to the majority of hydrodynamic models, the HYDJET++ model combines parametrized hydrodynamics with jets. Only second and third flow harmonics are generated at the freeze-out hypersurface in the present version of the model; therefore, the hexagonal flow originates solely as a result of nonlinear hydrodynamic response,  $v_6 \sim v_2^3 + v_3^2$ . The following conclusions can be drawn.

(1) Scaling of the ratio  $v_6^{1/6}\{\Psi_2\}/v_2^{1/2}\{\Psi_2\}$  is observed in the  $\Psi_2$  event plane within the indicated centrality interval. No scaling is found for the ratio  $v_6^{1/6}\{\Psi_3\}/v_3^{1/3}\{\Psi_3\}$ .

(2) Jets increase both ratios by 10%–15% and lead to rising high- $p_t$  tails at  $p_t \geq 3$  GeV/c.

(3) The behavior of the plane correlators  $\langle \cos 6(\Psi_2 - \Psi_6) \rangle$  and  $\langle \cos 6(\Psi_3 - \Psi_6) \rangle$  is in line with the experimental observations and with the centrality dependencies of  $v_6$  on  $v_2$  and  $v_3$  in the  $\Psi_2$  and  $\Psi_3$  event planes, respectively. These findings strongly favor the idea that basic features of the hexagonal flow can be understood as a result of contributions of elliptic and triangular flows and their interplay. Original hexagonal initial fluctuations seem to play a minor role in the formation of  $v_6$ .

*Acknowledgments.* Fruitful discussions with L. Csernai and J.-Y. Ollitrault are gratefully acknowledged. This work was supported in parts by the Department of Physics, UiO, Russian Foundation for Basic Research under Grant No. 12-02-91505 and a Grant of the President of Russian Federation for Scientific School Supporting No. 3920.2012.2.

- 
- [1] I. Arsene *et al.* (BRAHMS Collaboration), Nucl. Phys. A **757**, 1 (2005); B.B. Back *et al.* (PHOBOS Collaboration), *ibid.* **757**, 28 (2005); J. Adams *et al.* (STAR Collaboration), *ibid.* **757**, 102 (2005); K. Adcox *et al.* (PHENIX Collaboration), *ibid.* **757**, 184 (2005).
  - [2] E. Shuryak, Prog. Part. Nucl. Phys. **53**, 273 (2004).
  - [3] J.-Y. Ollitrault, Phys. Rev. D **46**, 229 (1992); **48**, 1132 (1993).
  - [4] S. A. Voloshin, A. M. Poskanzer, and R. Snellings, in *Relativistic Heavy Ion Physics*, Landolt-Börnstein Database Vol. 23, edited by R. Stock (Springer, Berlin, 2010), p.5–54.
  - [5] M. Bleicher and H. Stöcker, Phys. Lett. B **526**, 309 (2002).
  - [6] E. E. Zabrodin, C. Fuchs, L. V. Bravina, and Amand Faessler, Phys. Lett. B **508**, 184 (2001).
  - [7] G. Burau, J. Bleibel, C. Fuchs, Amand Faessler, L. V. Bravina, and E. E. Zabrodin, Phys. Rev. C **71**, 054905 (2005).
  - [8] H. Song, S. A. Bass, and U. Heinz, Phys. Rev. C **83**, 024912 (2011).
  - [9] B. Schenke, S. Jeon, and C. Gale, Phys. Rev. C **82**, 014903 (2010).
  - [10] S. Voloshin and Y. Zhang, Z. Phys. C **70**, 665 (1996).
  - [11] A. M. Poskanzer and S. A. Voloshin, Phys. Rev. C **58**, 1671 (1998).
  - [12] J. Velkovska *et al.* (CMS Collaboration), J. Phys. G **38**, 124011 (2011); J. Jia *et al.* (ATLAS Collaboration), *ibid.*

- 38**, 124012 (2011); R. Snellings *et al.* (ALICE Collaboration), *ibid.* **38**, 124013 (2011).
- [13] B. Alver and G. Roland, Phys. Rev. C **81**, 054905 (2010).
- [14] B. H. Alver, C. Gombeaud, M. Luzum, and J.-Y. Ollitrault, Phys. Rev. C **82**, 034913 (2010).
- [15] G.-Y. Qin, H. Petersen, S. A. Bass, and B. Müller, Phys. Rev. C **82**, 064903 (2010).
- [16] F. G. Gardim, F. Grassi, M. Luzum, and J.-Y. Ollitrault, Phys. Rev. C **85**, 024908 (2012).
- [17] Z. Qiu and U. Heinz, Phys. Rev. C **84**, 024911 (2011).
- [18] D. Teaney and L. Yan, Phys. Rev. C **86**, 044908 (2012).
- [19] U. Heinz and R. Snellings, Annu. Rev. Nucl. Part. Sci. **64**, 123 (2013).
- [20] I. P. Lokhtin, L. V. Malinina, S. V. Petrushanko, A. M. Snigirev, I. Arsene, and K. Tywoniuk, Comput. Phys. Commun. **180**, 779 (2009).
- [21] N. S. Amelin, R. Lednicky, T. A. Pocheptsov, I. P. Lokhtin, L. V. Malinina, A. M. Snigirev, Iu. A. Karpenko, and Yu. M. Sinyukov, Phys. Rev. C **74**, 064901 (2006).
- [22] N. S. Amelin, R. Lednicky, I. P. Lokhtin, L. V. Malinina, A. M. Snigirev, Iu. A. Karpenko, Yu. M. Sinyukov, I. Arsene, and L. Bravina, Phys. Rev. C **77**, 014903 (2008).
- [23] I. P. Lokhtin and A. M. Snigirev, Eur. Phys. J. **C46**, 211 (2006).
- [24] <http://cern.ch/lokhtin/pyquen>.
- [25] K. Tywoniuk, I. C. Arsene, L. Bravina, A. B. Kaidalov, and E. Zabrodin, Phys. Lett. B **657**, 170 (2007).
- [26] L. V. Bravina, B. H. Brusheim Johansson, G. Kh. Eyyubova, V. L. Korotkikh, I. P. Lokhtin, L. V. Malinina, S. V. Petrushanko, A. M. Snigirev, and E. E. Zabrodin, arXiv:1311.7054.
- [27] B. Abelev *et al.* (ALICE Collaboration), Phys. Rev. Lett. **111**, 232302 (2013).
- [28] C. Gombeaud and J.-Y. Ollitrault, Phys. Rev. C **81**, 014901 (2010).
- [29] L. Bravina, B. H. Brusheim Johansson, G. Eyyubova, and E. Zabrodin, Phys. Rev. C **87**, 034901 (2013).
- [30] E. Zabrodin, G. Eyyubova, L. Malinina, and L. Bravina, Acta Phys. Pol. B Proc. Suppl. **5**, 349 (2012).
- [31] N. Borghini and J.-Y. Ollitrault, Phys. Lett. B **642**, 227 (2006).
- [32] G. Aad *et al.* (ATLAS Collaboration), Phys. Rev. C **86**, 014907 (2012).
- [33] S. Chatrchyan *et al.* (CMS Collaboration), Phys. Rev. C **87**, 014902 (2013).
- [34] G. Eyyubova, L. V. Bravina, E. E. Zabrodin, V. L. Korotkikh, I. P. Lokhtin, L. V. Malinina, S. V. Petrushanko, and A. M. Snigirev, Phys. Rev. C **80**, 064907 (2009).
- [35] E. Zabrodin, G. Eyyubova, L. Bravina, I. P. Lokhtin, L. V. Malinina, S. V. Petrushanko, and A. M. Snigirev, J. Phys. G. **37**, 094060 (2010).
- [36] S. Chatrchyan *et al.* (CMS Collaboration), arXiv:1310.8651.
- [37] R. S. Bhalerao, M. Luzum, and J.-Y. Ollitrault, Phys. Rev. C **84**, 034910 (2011).
- [38] J. Jia *et al.* (ATLAS Collaboration), Nucl. Phys. A **910-911**, 276 (2013).
- [39] R. S. Bhalerao, J.-Y. Ollitrault, and S. Pal, Phys. Rev. C **88**, 024909 (2013).